

**Evolution of anisotropic-to-isotropic photoexcited carrier distribution in graphene**Xiao-Qing Yan,<sup>1,2</sup> Jun Yao,<sup>1</sup> Zhi-Bo Liu,<sup>1,\*</sup> Xin Zhao,<sup>1,3</sup> Xu-Dong Chen,<sup>1</sup> Chengmin Gao,<sup>1</sup> Wei Xin,<sup>1</sup> Yongsheng Chen,<sup>2</sup> and Jian-Guo Tian<sup>1,†</sup><sup>1</sup>*The Key Laboratory of Weak Light Nonlinear Photonics, Ministry of Education, Teda Applied Physics Institute and School of Physics, Nankai University, Tianjin 300457, China*<sup>2</sup>*The Key Laboratory of Functional Polymer Materials and Center for Nanoscale Science and Technology, Institute of Polymer Chemistry, College of Chemistry, Nankai University, Tianjin 300071, China*<sup>3</sup>*College of Science, Tianjin Polytechnic University, Tianjin 300387, China*

(Received 16 May 2014; published 17 October 2014)

Femtosecond degenerate and nondegenerate pump-probe spectroscopy in graphene reveals the evolution of photoexcited carrier distribution in the energy band during relaxation: the initial occupation of photoexcited carriers centered at the excitation state is anisotropic in momentum space; this anisotropic distribution rapidly relaxes through an intermediate state argued to be fully isotropic in the energy band due to phonon-involved cascade scattering. In addition, the experiment suggests that graphene optical absorbances for in-plane and out-of-plane optical fields are identical.

DOI: [10.1103/PhysRevB.90.134308](https://doi.org/10.1103/PhysRevB.90.134308)

PACS number(s): 78.67.Wj, 72.20.Jv, 78.47.jh, 78.20.Ci

The nearly linear electronic band structure at the Dirac point gives rise to remarkable electrical and optical properties for graphene [1–4], which make it a promising candidate for novel optoelectronic and photonic devices [5]. The redistribution of photoexcited charge carriers in energy and momentum space is the most important process, as it governs the transient optical response (e.g., optical absorption and light emission) of graphene [6–8]. Understanding the nonequilibrium carrier distribution evolution with relaxation is of capital importance for the implementation of graphene-based optoelectronic devices and is of fundamental interest [2,3,7,9].

It is predicted that the momentum spatial occupation of graphene photoexcited carriers maximizes in the direction perpendicular to the light polarization due to the optical matrix element describing resonant excitation as anisotropic [10,11]. Time- and angle-resolved photoemission spectroscopy is an efficient technique of mapping the carrier distribution and is successfully used to verify the occurrence of population inversion [12] and carrier multiplication [13] in graphene [2,14,15]. However, a direct mapping of the nonequilibrium carrier distribution in the Dirac cones with this technique is limited by the difficulty of femtosecond (fs) photoemission experiments to reach certain parts of the Brillouin zone. In a graphene pump-probe measurement, the Pauli blocking caused differential reflectivity and transmittance ( $\Delta R/R$  and  $\Delta T/T$ , a result of a decrease in optical conductivity  $\Delta\sigma$  or extinction coefficient  $\Delta k$ ) signal intensity reflects the carrier occupation profile at the optically probed state [16,17]. Owing to the fact that photoexcited carrier distribution is directly determined by pump polarization [10], studying the pump polarization dependence of the  $\Delta R/R$  signal intensity by using degenerate measurement could reveal the photoexcited carrier distribution at the excitation state. Similarly, using probe pulses with lower or higher photon energy, we could determine the distribution of carriers scattered from the excitation state. Therefore, the carrier distribution evolution can be very effectively

studied with polarized light pump-probe spectroscopy. Using degenerate measurement, Mittendorff *et al.* have reported that the initial photoexcited carrier distribution at a state of 0.775 eV is anisotropic; they showed that in the first tens of fs, where carrier-carrier (CC) scattering dominated the dynamics, the carrier distribution remained anisotropic [18]. Subsequent carrier-phonon (CP) scattering lead to an isotropic distribution within 150 fs. As we know, the initial photoexcited carriers centered at the excitation state are immediately spread over the energy band by carrier thermalization (CT) and then cool to the Dirac point by CP scattering. So far, little is known about the evolution of nonequilibrium carrier distribution in such a unique energy band during relaxation, such as the distribution evolution of carriers created by scattering.

Prior graphene optical absorbance studies have been mostly concerned with the in-plane optical field (we will use  $k_{\parallel}$  to describe this optical absorbance) [19,20]; the optical absorbance for the out-of-plane optical field ( $k_{\perp}$ ) is not well measured [21]. Determining such anisotropy from transmittance and reflection of obliquely incident light requires removing the suppression of polarization dependent linear transmittance and reflection on the measured absorption signal, yet such measurement has been overlooked so far. Spectroscopy ellipsometry measurement is not suitable for studying this anisotropy due to the fact that the sensitivity of an ellipsometry measurement to such anisotropy is limited by graphene thinness [21]. During graphene optical absorption, the photoexcited carrier density is proportional to the absorbed fluence [5]. In return, graphene optical absorption properties could be inferred from the photoexcited carrier density [3], which could determine the  $\Delta R/R$  signal. Thus, pump-probe spectroscopy offers us an alternative pathway to compare  $k_{\parallel}$  and  $k_{\perp}$  from the dependence of photoexcited carrier density on the polarization of the obliquely incident pump beam.

Here, we present both degenerate and nondegenerate pump-probe spectroscopy in graphene, revealing the evolution of photoexcited carrier distribution at different energy states in the energy band. Remarkable pump polarization dependence was observed in the degenerate  $\Delta R/R$  signal during photoexcitation, suggesting the creation of an anisotropic distribution

\*rainingstar@nankai.edu.cn

†jjtian@nankai.edu.cn

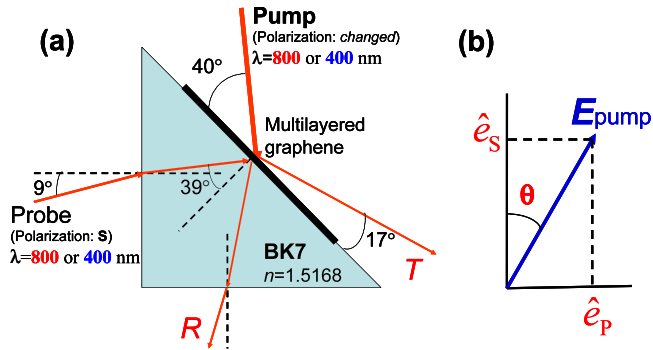


FIG. 1. (Color online) (a) Experimental configuration. (b) Polarization orientation of the linearly polarized pump beam.

of carriers. During carrier cooling, the  $\Delta R/R$  was found to be completely independent of the pump polarization from both degenerate and nondegenerate measurements, reflecting the isotropic distribution of hot carriers in the energy band. In addition, we deduce that the graphene absorbance is isotropic for 400- and 800-nm light from the independence of  $\Delta R/R$  on polarization of the obliquely incident pump beam. This work presents an experimental observation of the symmetry evolution of the photoexcited carrier distribution in the graphene energy band and provides valuable information about graphene optical absorption.

The experiment was performed with a mode-locked Ti-sapphire laser producing pulses at 800-nm wavelength; 800- and 400-nm (obtained by frequency doubling of 800-nm pulses) degenerate pump-probe measurements were used to approve the anisotropic distribution of photoexcited carriers and to monitor the distribution evolution at the excitation state, while the 400-nm pump, 800-nm probe and the 800-nm pump, 400-nm probe measurements were used to exemplify the scattering-created carrier distribution evolution at states with energies much lower and higher than the excitation state, respectively. As shown in Fig. 1(a), the probe beam was coming from the nontotal internal reflection at the interface between the graphene layer and a prism, and the pump beam was obliquely incident into the graphene sample (identical results were obtained for the normally incident pump beam; see S1 in [22]). It should be noted that this configuration is without special aim; the reported pump polarization dependence of  $\Delta R/R$  (or  $\Delta T/T$ ) in this paper could also be observed in the other configuration (on the other substrate and incident into graphene with another angle; e.g., see S2 in [22]). We used two  $\lambda/2$  plate, Glan Taylor prism, and  $\lambda/2$  plate combinations to alter the polarization orientation [Fig. 1(b)] and fluence of the linearly polarized probe and pump beams. The probe polarization was *S* in the experiment presented here (for the case of the *p*-polarized probe beam, see S3 in [22]). Although the temporal resolution ( $\sim 424$  and  $325$  fs for 800- and 400-nm degenerate measurement, respectively; see S4 in [22]) is much larger than the CT time (within 40 fs [2,15]), the conclusions obtained from the pump polarization dependence rather than relaxation time of  $\Delta R/R$  are reliable. To study carrier distribution evolution and compare optical absorbance, we need only focus on the pump polarization and fluence dependence of  $\Delta R/R$  probed with a certain polarized beam (see S5 in [22] for the probe polarization dependence).

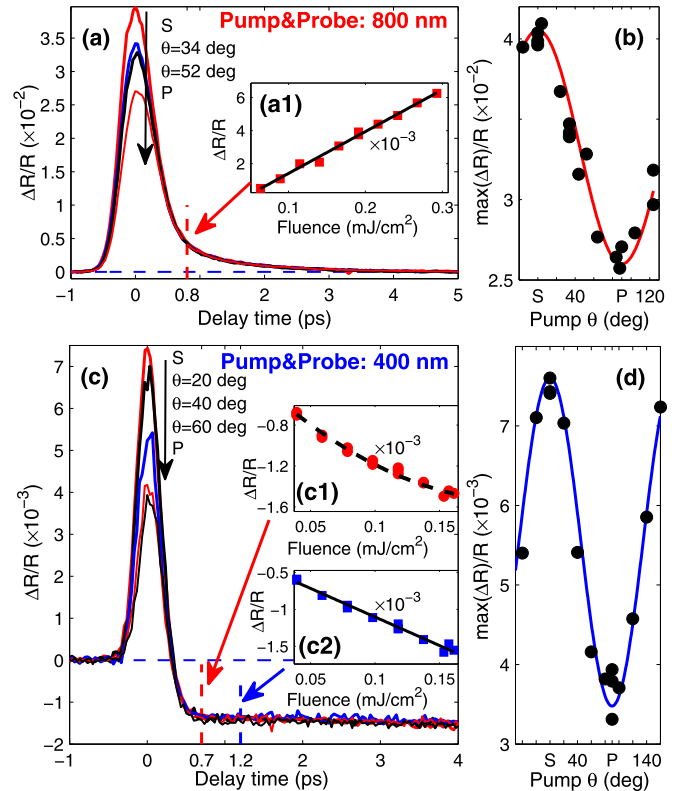


FIG. 2. (Color online) Pump polarization dependent  $\Delta R/R$  time traces for degenerate cases. (a1), (c1), and (c2) Pump fluence dependence of ps dynamics signal. We choose the  $\Delta R/R$  at a delay time of 0.83 ps in (a1) and 0.7 ps in (c1) as representative of the ps dynamics signal; the choice is to exclude the influence of the autocorrelation signal. The solid lines in (a1) and (c2) are linear fits; the dashed line in (b1) is a quadratic fit. The  $\Delta R/R$  at longer decay time ( $\geq 1.2$  ps) scales linearly with pump fluence. The decay times of the ps dynamics signal in (a) and (b) are  $1.1 \pm 0.1$  and  $80 \pm 8$  ps, respectively. (b) and (d) Peak  $\Delta R/R$  vs angle  $\theta$  for (b) 800-nm and (d) 400-nm optical excitation; solid lines are fits. The  $\Delta R/R$  time scan measured with a 3.1-eV photon agrees with that probed with a 3.2-eV photon in [26] (the 3.1-eV photon-probed  $\Delta R/R$  at long delay time is shown in S7 of [22]).

A chemical vapor deposition (CVD) multilayered graphene (approximately five graphene layers) was used in the experiment. Such multilayered graphene has electronic properties similar to those of a monolayer and without interlayer coupling (see [23,24] and S6 in [22]); the laser spot of the probe beam at graphene was  $\sim 35$   $\mu\text{m}$ , covering multiple graphene flakes [23–25]. We verified that the measurement on different graphene samples yielded similar results. Since the crystalline orientation in CVD graphene is disordered, the similar results indicate no influence of crystalline orientation on such polarization dependence [24,25], which agrees well with the former report [18]. The pump polarization dependence of  $\Delta R/R$  has also been observed in CVD monolayer graphene (see S1 in [22]).

Figure 2 shows the representative pump polarization and fluence dependent ultrafast degenerate  $\Delta R/R$  spectroscopy. Pronounced pump polarization dependence is observed for  $\Delta R/R$  around zero delay time, i.e., carrier generation and

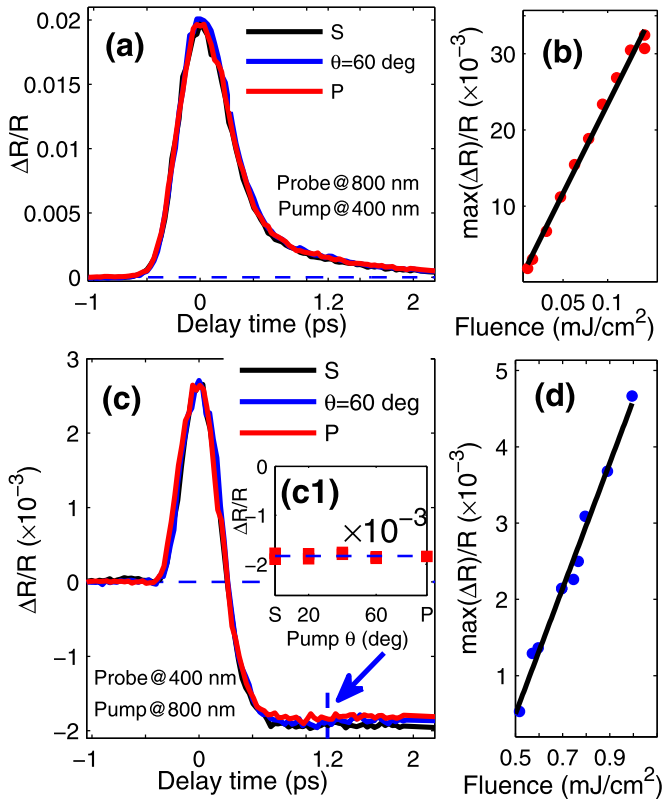


FIG. 3. (Color online) (a) and (c) Polarization independent  $\Delta R/R$  time traces for nondegenerate cases. Zero delay corresponds to the maximum pump-probe signal. (c1) Zoom in view of pump polarization independence of  $\Delta R/R$ . (b) and (d) Pump fluence dependence of peak  $\Delta R/R$  for cases of the (b) 400-nm pump and 800-nm probe and (d) 800-nm pump and 400-nm probe; solid lines are linear fits. The decay times of the ps dynamics signal in (a) and (b) are  $1.2 \pm 0.2$  and  $115 \pm 10$  ps, respectively.

initial relaxation processes. If pump polarization is parallel or perpendicular to the probe polarization, the peak  $\Delta R/R$  signal is maximum or minimum, respectively. With carrier relaxation, the pump polarization dependence rapidly vanishes; no polarization dependence is observed in the picosecond (ps) dynamic signal (i.e., the  $\Delta R/R$  signal with decay time in the ps time scale, corresponding to the carrier cooling process [5]). The observed pump polarization dependence of  $\Delta R/R$  could not originate from anisotropy of Fresnel reflection due to the following.

(1) Similar pump polarization dependence also applies to the case with the  $p$ -polarized probe beam (see S3 in [22]). The peak  $\Delta R/R$  signal maximizes or minimizes when the pump polarization is parallel or perpendicular to probe polarization, respectively, and there is no pump polarization dependence in the ps dynamics signal.

(2) Quite consistent pump polarization dependence of  $\Delta R/R$  was observed when the pump beam was normally incident into the sample (see S1 in [22]). For normally incident light, the reflection is polarization independent in graphene [21,27].

(3) There was no pump polarization dependence in our nondegenerate signal (Fig. 3). If the pump polarization

dependence does stem from anisotropic reflection, we could not obtain these results.

When the pump beam is incident into extremely thin graphene layers (thickness is 1–2 nm) from air, the light intensity in graphene layers is close to that of incident light intensity and nearly identical for different polarized incident light [21,27]. The polarization dependence of  $\Delta R/R$  must arise from the intrinsic optical property of graphene.

For the two degenerate cases, the ps dynamics signal changes with pump fluence, which determines the photoexcited carrier density (i.e., the ps dynamics signal depends on photoexcited carrier density), but does not change with pump polarization no matter the probe polarization (Fig. 2 and S3 in [22]). The possibility that the independence of the ps dynamics signal on pump polarization is caused by combined action of anisotropic optical absorption and anisotropic carrier distribution could be precluded, for the following reason: if the optical absorption is polarization dependent, to guarantee that the ps dynamics signal probed with the  $s$ -polarized beam is pump polarization independent the distribution of carriers in the ps dynamics process should monotonously change from a direction parallel to pump polarization to one perpendicular to pump polarization [28]. Also, the pump polarization dependence induced by this anisotropic distribution profile is opposite to that caused by the hot carrier density for the  $s$ -polarized probe beam. For the  $p$ -polarized probe beam, the pump polarization dependence of  $\Delta R/R$  caused by the hot carrier density is identical to that probed with the  $s$ -polarized beam (see S3 and S5 in [22]), but this anisotropic distribution profile will result in similar pump polarization dependence of  $\Delta R/R$  as that caused by the hot carrier density according to light-carrier interaction (i.e., pump polarization dependence caused by this anisotropic distribution profile is opposite for the  $s$ - and  $p$ -polarized probe beams) [28]. Thus, the ps dynamics signal probed with the  $p$ -polarized beam could not be pump polarization independent, which is opposite to the experiment. Therefore, we can conclude that the carrier distribution in the ps dynamics process is isotropic and the density of carriers generated by the different polarized pump beam is identical;  $k_{\perp}$  is equal to  $k_{\parallel}$ . We note that the isotropic optical absorbance concluded here is not consistent with theoretical prediction (namely,  $k_{\perp} = 0$  for a photon energy smaller than 7.5 eV) [29]. Indeed, the  $k_{\perp}$  of graphite has also been debated in the visible region of the spectrum [29–31]. The  $k_{\perp}$  of graphite was regarded from interlayer interaction and predicted to be much smaller than  $k_{\parallel}$  [29,31]; however, the measured  $k_{\perp}$  of graphite was relatively smaller than  $k_{\parallel}$  [30]. The pronounced optical absorption along the  $c$  axis could not be a result of interlayer interaction. These conflicts especially indicate the need for a theory valid all the way to optical absorption along the  $c$  axis in graphite and graphene.

Owing to the fact that the photoexcited carrier density is identical for the different polarized pump beam, the pump polarization dependence of  $\Delta R/R$  during photoexcitation should stem from the different occupation profile of carriers photoexcited by the different polarized pump beam. All the pump polarization dependence of  $\max(\Delta R/R)$  indicates that the momentum spatial occupation of photoexcited carriers is maximum or minimum in the direction perpendicular or parallel, respectively, to pump polarization [10]. Reduction in pump

polarization dependence of  $\Delta R/R$  with decay time reflects that this anisotropy in distribution reduces with relaxation and totally vanished in the cooling process. The electronic band curvature at 1.55 eV deviates significantly from isotropic due to trigonal warping [32]. It was predicted that relaxation for a range of directions of the initial carrier momentum was suppressed by the anisotropic energy band. As shown here, such suppression does not prohibit the anisotropic distribution rapidly evolving to isotropic [Figs. 2(c) and 3(c)]. Under normally incident light excitation, the photoexcited carrier density is polarization independent due to isotropic optical absorption in the graphene plane [21]. The identical pump polarization dependence of  $\Delta R/R$  for normally incident light excitation further substantiates the physical picture discussed above (see S1 in [22]).

The dependence of  $\max(\Delta R)/R$  on  $\theta$  [Figs. 2(b) and 2(d)] could be well fitted by function  $\max(\Delta R)/R = \alpha(N \cos 2\theta + M)$  (see S8 in [22]),  $\alpha$  is a free parameter, and the two parameters  $N$  and  $M$  are defined as

$$N = \frac{\pi}{4} \int_{-\infty}^{+\infty} \int_{-\infty}^{+\infty} e^{-\left(\frac{t_{\text{pump}}}{\tau_p}\right)^2} \left( e^{-\frac{t_{\text{pump}} - t_{\text{probe}}}{\tau_1}} + A e^{-\frac{t_{\text{pump}} - t_{\text{probe}}}{\tau_2}} \right) \times e^{-\left(\frac{t_{\text{probe}}}{\tau_p}\right)^2} e^{-\frac{t_{\text{pump}} - t_{\text{probe}}}{\tau_{\text{aniso}}}} dt_{\text{probe}} dt_{\text{pump}}, \quad (1)$$

$$M = \frac{\pi}{2} \int_{-\infty}^{+\infty} \int_{-\infty}^{+\infty} e^{-\left(\frac{t_{\text{pump}}}{\tau_p}\right)^2} \left( e^{-\frac{t_{\text{pump}} - t_{\text{probe}}}{\tau_1}} + A e^{-\frac{t_{\text{pump}} - t_{\text{probe}}}{\tau_2}} \right) \times e^{-\left(\frac{t_{\text{probe}}}{\tau_p}\right)^2} dt_{\text{probe}} dt_{\text{pump}}, \quad (2)$$

where  $\tau_p = \tau_{\text{FWHM}}/(2\sqrt{\ln 2})$ ,  $\tau_1$  and  $\tau_2$  are the two decay times of carrier relaxation [2],  $A$  is a parameter describing the weight of the two types of relaxation, and  $\tau_{\text{aniso}}$  is the decay time of anisotropy which is assumed to relax in an exponential function as in silicon [33]. From fitting,  $\tau_{\text{aniso}}$  is determined to be  $\sim 45$  fs at an energy state of 0.775 eV, which is in broad agreement with the former report (the fully vanished time of 150 fs is corresponding to  $\tau_{\text{aniso}} \approx 30$  fs) [18]. The peak  $\Delta R/R$  ratio of parallel to perpendicular polarization is  $(M + N)/(M - N)$ , which could be enlarged by using shorter pulses (see S8 in [22]). The ratio is  $1.4 \pm 0.2$  and  $2 \pm 0.2$  for 800- and 400-nm optical excitation, respectively. One reason for the larger ratio for 400-nm optical excitation is the shorter width of 400-nm pulses; another possible reason is the suppression of carrier relaxation at an energy state of 1.55 eV [32], which further increases the ratio value.

Now we turn to the distribution of carriers created by scattering at states with energy half (400-nm pump and 800-nm probe) and double (800-nm pump and 400-nm probe) the excitation energy. The typical  $\Delta R/R$  time traces are shown in Fig. 3. For the two nondegenerate cases, no visible pump polarization dependence is observed in the entire  $\Delta R/R$  time trace, and the peak  $\Delta R/R$  scales linearly with pump fluence. Thus, the possibility that carriers at an energy state of 1.55 eV are driven by a two-photon absorption process could be ruled out in the case of 800-nm optical excitation [34]. For both nondegenerate cases, these monitored carriers are created by scattering of one-photon excited carriers. During the initial rise of  $\Delta R/R$ , the ‘‘nonthermal’’ carriers centered at the excitation state are spread over a wide energy range (both upper and

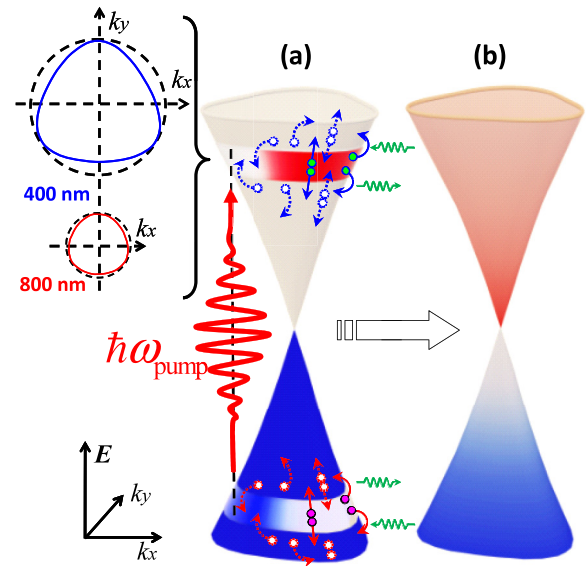


FIG. 4. (Color online) Schematic illustration of the photoexcited carrier distribution evolution in the graphene electronic band structure. The red and white color of the conical surface indicates carrier occupation density in the conduction and valence band, respectively. (a) The anisotropic distribution of carriers generated by a linearly polarized beam and potential scattering pathway for carriers (the dotted arrows indicate secondary scattering channels for the photoexcited carriers scattered from the excitation state). (b) Isotropic carrier distribution. Upper left inset: Electronic band curvature for excitation of 400-nm and 800-nm pulses.

lower energy states) via CT. As a consequence, the effective temperature of carrier distribution increases and reaches the peak value when a Fermi-Dirac distribution is established [3,35]. Correspondingly, the carrier population at the optically probed state is maximum and  $\Delta R/R$  reaches the peak value [28]. Subsequent CP scattering dominates carrier cooling and governs the decrease of  $\Delta R/R$  [3].

As peak  $\Delta R/R$  linearly depends on pump fluence, pump polarization independence of  $\Delta R/R$  indicates identical photoexcited carrier density for the different polarized pump beam (the  $C_4$  symmetrical carrier relaxation pathway could be excluded from the  $C_3$  symmetry of the graphene electronic band structure, so the amount of hot carriers scattered to any energy state is independent of pump polarization). This means the optical absorbances for in-plane and out-of-plane optical fields are identical (i.e.,  $k_{\parallel} = k_{\perp}$ ). Accordingly, isotropic optical absorbance of graphene at 800 and 400 nm is further substantiated. Based on the band structure and broadband optical absorbance of graphene [19], isotropic optical absorbance in the optical frequency range could be predicted.

Pump polarization independence of  $\Delta R/R$  reveals that the carrier distribution at monitored states is fully isotropic in the entire relaxation process. The initial anisotropy at the excitation state rapidly reduces when carriers are being scattered to another energy state (Fig. 4). After adequate relaxation, the carrier distribution is fully isotropic in the whole energy band. Then the isotropic distributed hot carriers cool to the Dirac point. If the energy state is away from the excitation state, such as the energy states optically probed here (the cases in Fig. 3), the distribution of hot carriers is fully isotropic in the entire

nonequilibrium process. Now we can understand why the photoluminescence is unpolarized in graphene [36]. The redistribution of nonthermal carrier momentum implies that the initial carrier relaxation is anisotropic in the Dirac cones (Fig. 4).

CC and CP scatterings are two competing relaxation channels in graphene [28]. Under the requirement of both energy and momentum conservations, CC scattering in graphene favors a collinear pattern (along the Dirac cone) in the nearly linear energy band [34,35]. In contrast, CP scattering could bring the carrier across the Dirac cone due to the relatively dispersive momentum of the phonon [10]. In the nearly linear energy band, the contribution of CC scattering to the rapid anisotropy reduction is finite [28]. Therefore, CP scattering is primarily responsible for redistributing the momentum of photoexcited carriers [10]. A recent microscopic simulation by Malic *et al.* strongly supports the carrier distribution evolution and suggests that the anisotropy reduction is a direct consequence of interaction of carriers with phonons in graphene [10,13,28]. As shown in the nondegenerate cases (Fig. 3), this anisotropy completely vanishes when the photoexcited carriers are scattered to an energy state away from the excitation state; thus, the CP scattering should take part in CT. Detailed theoretical analysis suggests that the  $\Gamma$ - $E_{2g}$  LO phonon ( $\sim 200$  meV) contributes significantly to the anisotropy reduction [13]. Since the energy difference between the excitation state and monitored energy state (0.775 eV) in the nondegenerate case is larger than the phonon energy, one step CP scattering could not realize the rapid transition from the excitation state to our monitored states. We therefore conclude that phonon-involved cascade scattering has contributed to the distribution evolution (Fig. 4). The unexpected isotropic distribution of dense hot carriers at a state of 1.55 eV [Fig. 3(b)]

implies that this cascade scattering is very efficient in promoting carriers to an energetically higher state during CT.

In summary, degenerate and nondegenerate pump-probe spectroscopy has been performed to study the photoexcited charge-carrier distribution evolution at different energy states in graphene and to compare graphene optical absorbance for in-plane and out-of-plane optical fields. Two important conclusions are obtained.

(1) The initial occupation of photoexcited carriers centered at the excitation state is anisotropic in momentum space. This anisotropic distribution quickly evolves to fully isotropic in the energy band via phonon-involved cascade scattering. Also, the distribution of scattering-created carriers at an energy state away from the excitation state is isotropic in the entire nonequilibrium process.

(2) Graphene optical absorbances for in-plane and out-of-plane optical fields are suggested to be identical.

Understanding of graphene optical absorbance and photoexcited carrier distribution evolution opens the possibility of exploring polarization and incidence-angle insensitive graphene-based optoelectronic devices and manipulating graphene's instantaneous optical response.

The authors would like to acknowledge helpful discussions with Prof. Fabrizio Carbone, Dr. Ermin Malic, and Dr. Martin Mittendorff. This work was supported by the Chinese National Key Basic Research Special Fund (Grant No. 2011CB922003), International Science and Technology Cooperation Program of China (Grant No. 2013DFA51430), National Natural Science Foundation of China (Grants No. 11174159, No. 11374164, and No. 11304166) and Fundamental Research Funds for the Central Universities (Grant No. 65145005).

- 
- [1] S. F. Shi, T. T. Tang, B. Zeng, L. Ju, Q. Zhou, A. Zettl, and F. Wang, *Nano Lett.* **14**, 1578 (2014).
- [2] I. Gierz, J. C. Petersen, M. Mitrano, C. Cacho, I. C. E. Turcu, E. Springate, A. Stohr, A. Kohler, U. Starke, and A. Cavalleri, *Nature Mater.* **12**, 1119 (2013).
- [3] K. J. Tielrooij, J. C. W. Song, S. A. Jensen, A. Centeno, A. Pesquera, A. Zurutuza Elorza, M. Bonn, L. S. Levitov, and F. H. L. Koppens, *Nature Phys.* **9**, 248 (2013).
- [4] F. Carbone, G. Aubock, A. Cannizzo, F. Van Mourik, R. R. Nair, A. K. Geim, K. S. Novoselov, and M. Chergui, *Chem. Phys. Lett.* **504**, 37 (2011).
- [5] L. B. Huang, G. V. Hartland, L. Q. Chu, Luxmi, R. M. Feenstra, C. X. Lian, K. Tahy, and H. L. Xing, *Nano Lett.* **10**, 1308 (2010).
- [6] T. Limmer, J. Feldmann, and E. Da Como, *Phys. Rev. Lett.* **110**, 217406 (2013).
- [7] P. A. Obraztsov, M. G. Rybin, A. V. Tyurnina, S. V. Garnov, E. D. Obraztsova, A. N. Obraztsov, and Y. P. Svirko, *Nano Lett.* **11**, 1540 (2011).
- [8] B. A. Ruzicka, S. Wang, J. W. Liu, K. P. Loh, J. Z. Wu, and H. Zhao, *Opt. Mater. Express* **2**, 708 (2012).
- [9] J. H. Strait, H. N. Wang, S. Shivaraman, V. Shields, M. Spencer, and F. Rana, *Nano Lett.* **11**, 4902 (2011).
- [10] E. Malic, T. Winzer, and A. Knorr, *Appl. Phys. Lett.* **101**, 213110 (2012).
- [11] B. Y. Sun and M. W. Wu, *New J. Phys.* **15**, 083038 (2013).
- [12] T. Li, L. Luo, M. Hupalo, J. Zhang, M. C. Tringides, J. Schmalian, and J. Wang, *Phys. Rev. Lett.* **108**, 167401 (2012).
- [13] E. Malic and A. Knorr, *Graphene and Carbon Nanotubes: Ultrafast Relaxation Dynamics and Optics* (Wiley, New York, 2013).
- [14] L. I. Johansson, R. Armiento, J. Avila, C. Xia, S. Lorcy, I. A. Abrikosov, M. C. Asensio, and C. Virojanadara, *Sci. Rep.* **4**, 4157 (2014).
- [15] J. C. Johannsen, S. Ulstrup, F. Cilento, A. Crepaldi, M. Zacchigna, C. Cacho, I. C. E. Turcu, E. Springate, F. Fromm, C. Raidel, T. Seyller, F. Parmigiani, M. Grioni, and P. Hofmann, *Phys. Rev. Lett.* **111**, 027403 (2013).
- [16] J. Z. Shang, T. Yu, J. Y. Lin, and G. G. Gurzadyan, *ACS Nano* **5**, 3278 (2011).
- [17] M. M. Leandro, M. Kin Fai, A. H. C. Neto, N. M. R. Peres, and F. H. Tony, *New J. Phys.* **15**, 015009 (2013).
- [18] M. Mittendorff, T. Winzer, E. Malic, A. Knorr, C. Berger, W. A. de Heer, H. Schneider, M. Helm, and S. Winnerl, *Nano Lett.* **14**, 1504 (2014).
- [19] K. F. Mak, M. Y. Sfeir, Y. Wu, C. H. Lui, J. A. Misewich, and T. F. Heinz, *Phys. Rev. Lett.* **101**, 196405 (2008).

- [20] A. B. Kuzmenko, E. van Heumen, F. Carbone, and D. van der Marel, *Phys. Rev. Lett.* **100**, 117401 (2008).
- [21] F. J. Nelson, V. K. Kamineni, T. Zhang, E. S. Comfort, J. U. Lee, and A. C. Diebold, *Appl. Phys. Lett.* **97**, 253110 (2010).
- [22] See Supplemental Material at <http://link.aps.org/supplemental/10.1103/PhysRevB.90.134308> for more experimental data and analysis.
- [23] C.-C. Lu, C. Jin, Y.-C. Lin, C.-R. Huang, K. Suenaga, and P.-W. Chiu, *Langmuir* **27**, 13748 (2011).
- [24] A. Reina, X. Jia, J. Ho, D. Nezich, H. Son, V. Bulovic, M. S. Dresselhaus, and J. Kong, *Nano Lett.* **9**, 30 (2008).
- [25] <https://graphene-supermarket.com>.
- [26] A. T. Roberts, R. Binder, N. H. Kwong, D. Golla, D. Cormode, B. J. LeRoy, H. O. Everitt, and A. Sandhu, *Phys. Rev. Lett.* **112**, 187401 (2014).
- [27] V. G. Kravets, A. N. Grigorenko, R. R. Nair, P. Blake, S. Anissimova, K. S. Novoselov, and A. K. Geim, *Phys. Rev. B* **81**, 155413 (2010).
- [28] E. Malic, T. Winzer, E. Bobkin, and A. Knorr, *Phys. Rev. B* **84**, 205406 (2011).
- [29] P. E. Trevisanutto, M. Holzmann, M. Côté, and V. Olevano, *Phys. Rev. B* **81**, 121405(R) (2010).
- [30] G. E. Jellison, J. D. Hunn, and H. N. Lee, *Phys. Rev. B* **76**, 085125 (2007).
- [31] A. G. Marinopoulos, L. Reining, A. Rubio, and V. Olevano, *Phys. Rev. B* **69**, 245419 (2004).
- [32] D. M. Basko, *Phys. Rev. B* **87**, 165437 (2013).
- [33] A. J. Sabbah and D. M. Riffe, *Phys. Rev. B* **66**, 165217 (2002).
- [34] W.-T. Liu, S. W. Wu, P. J. Schuck, M. Salmeron, Y. R. Shen, and F. Wang, *Phys. Rev. B* **82**, 081408 (2010).
- [35] D. Brida, A. Tomadin, C. Manzoni, Y. J. Kim, A. Lombardo, S. Milana, R. R. Nair, K. S. Novoselov, A. C. Ferrari, G. Cerullo, and M. Polini, *Nature Commun.* **4**, 1987 (2013).
- [36] C. H. Lui, K. F. Mak, J. Shan, and T. F. Heinz, *Phys. Rev. Lett.* **105**, 127404 (2010).